International Journal of Nanomedicine

Dovepress
open access to scientific and medical research

Open Access Full Text Article

ORIGINAL RESEARCH

Safety and efficacy of PLGA(Ag-Fe_3O_4)-coated dental implants in inhibiting bacteria adherence and osteogenic inducement under a magnetic field

This article was published in the following Dove Press journal:
International Journal of Nanomedicine

Yaping Yang[1,*]
Shuangshuang Ren[2,*]
Xuan Zhang[2]
Yijun Yu[1]
Chao Liu[3]
Jie Yang[2]
Leiying Miao[1]

[1]Department of Cariology and Endodontics, [2]Department of Periodontology, [3]Department of Orthodontics, Nanjing Stomatological Hospital, Medical School of Nanjing University, Nanjing, Jiangsu, China

*These authors contributed equally to this work

Introduction: The placement of dental implants is performed in a contaminated surgical field in the oral cavity, which may lead to implant failure. Bacterial adhesion and proliferation (*Streptococcus mutans*, *Porphyromonas gingivalis*) often lead to implant infections. Although Ag nanoparticles hold great promise for a broad spectrum of antibacterial activities, their runoff from dental implants compromises their antibacterial efficacy and potentially impairs osteoblast proliferation. Thus, this aspect remains a primary challenge and should be controlled.

Materials and methods: In this study, PLGA(Ag-Fe_3O_4) was modified on the implanted tooth surface and was characterized by transmission electron microscopy, X-ray diffraction, and Fourier transform infrared spectroscopy. The magnetic and antibacterial properties were also determined.

Results: Results showed that Ag successfully bonded with Fe_3O_4, and Ag-Fe_3O_4 not only exerted superparamagnetism but also exhibited antibacterial activity almost identical to silver nanoparticles (nano-Ag). The PLGA(Ag-Fe_3O_4) coating could significantly maintain the antibacterial activity and avoid bacterial adhesion to the implant. Compared with the blank control group, PLGA(Ag-Fe_3O_4) under magnetic field-coated samples had a significantly lower amount of colonized *S. mutans* ($P<0.01$). Osteoblast proliferation results showed that the coated samples did not exhibit cytotoxicity and could promote osteoblast proliferation as shown by MTT, alkaline phosphatase, and the nucleolar organizer region count.

Conclusion: We developed a novel Ag biologically compatible nanoparticle in this study without compromising the nano-Ag antibacterial activity, which provided continuous antibacterial action.

Keywords: Ag-Fe_3O_4, PLGA, dental implants, antibacterial property

Introduction

Dental implants are embedded in the gum, which is a contaminated surgical field. The microbial composition may lead to peri-implantitis. As a result of the host immune response to pathogenic bacteria, destruction of the tooth supporting tissues, in particular alveolar bone resorption,[1] may occur and then lead to the augmentation of the probing depth to form peri-implant pockets. These pockets provide an ideal environment for microorganism colonization, which causes inflammation and tissue destruction, and eventually lead to potential failure of the dental implant.[2] Bacterial adhesion ability is considered to be one of the principal factors in microbial reproduction, consequently forming and consolidating a biofilm on dental enamel, tooth root surfaces, and dental implants.[3,4] Periodontitis is one of the main causes of tooth loss in adults and is the primary reason for the need for dental implants in China.

Correspondence: Leiying Miao
Department of Cariology and Endodontics, Nanjing Stomatological Hospital, Medical School of Nanjing University, 30 Zhongyang Road, Nanjing, Jiangsu 210008, China
Tel/fax +86 25 8362 0212
Email miaoleiying80@163.com

Jie Yang
Department of Periodontology, Nanjing Stomatological Hospital, Medical School of Nanjing University, 30 Zhongyang Road, Nanjing, Jiangsu 210008, China
Tel/fax +86 25 8362 0206
Email dorothy0314@sina.com

submit your manuscript | www.dovepress.com
Dovepress
http://dx.doi.org/10.2147/IJN.S159860

Peri-implant pockets may yield up to 10^7 different types of bacteria, which are in direct contact with the pocket epithelium. In oral inflammatory diseases, the bacteria *Streptococcus mutans* is considered as the principal microorganism associated with the beginning and development of inflammation due to its properties of metabolizing sucrose into lactic acid, synthesizing acids in a low pH environment, and producing extracellular and intracellular polysaccharides, which in turn promote further bacterial growth.[5,6] Bacterial adhesion on the surface of the teeth strongly improves bacteria–bacteria and bacteria–surface interconnection and consequently improves the adhesion and attachment of other microorganisms.[7] Furthermore, bacteria and their products are able to alter osteoblast proliferation, thus resulting in implant failure.[8,9]

Due to the complexity of the bacterial components, broad spectrum antibacterial action is important, and the usage of prophylactic antibiotics during implant placement remains indispensable. In the last few decades, researchers have focused their attention on silver nanoparticles (nano-Ag), which have shown broad spectrum antibacterial activity against various bacteria strains, including *Streptococcus*.[10] Some mechanisms of this antibacterial action have been revealed, such as silver causing bacterial cell death by interfering with DNA replication, alteration of the bacterial peptides profile, increasing permeability, and interacting with thiol groups.[11] Despite such potential, widespread use of nano-Ag is limited, primarily because of unwanted side effects. Due to the runoff from the working point, dose escalation is usually adopted to prolong the action time of nano-Ag. In contrast to molecular agents, nano-Ag usually accumulates in the reticuloendothelial system (ie, liver and spleen), resulting in hepatic and renal injuries.[12] Additionally, a high nano-Ag concentration may not result in osteoblast proliferation, which may decrease the survival rate of dental implants.[13] It is therefore important to enhance antibacterial activity and reduce bacterial adhesion ability without compromising biocompatibility.

Recently, the combination of noble metals and magnetic materials has attracted much attention,[14] such as Ag-modified magnetic particles that achieved very high sensitivity for compounds dissolved in solutions using magnetic capture.[15] Magnetic nanoparticles (Fe_3O_4) coupled with an active noble metal, such as silver (Ag-Fe_3O_4), result in a wide spectrum of desirable synergistic and complementary effects.[16] Despite these promising effects, in the case of dental implants, the problem of biocompatibility is yet to be solved. Magnetite colloids are superparamagnetic and biocompatible,[17] and nano-Ag is well known for its bactericide effect, potentially indicating a solution in regard to biosafety. Magnetic drug targeting employed nanoparticles as carriers, offering a promising treatment modality that avoids the side effects of conventional chemotherapy.[14] The antibacterial activity of Ag-Fe_3O_4 against both Gram-positive and Gram-negative pathogens has been reported.[18] In addition, paramagnetic implants can enhance the osteogenic response of pre-osteoblast cells.[19]

The healing of gums consists of an orderly series of events, such as osteoblast migration, proliferation, differentiation, and the formation of an extracellular matrix.[20] There is a considerable challenge to find an agent that improves both antibacterial activity and biocompatibility.[21] Inspired by the unique properties of Ag-Fe_3O_4 nanoparticles, we demonstrated the feasibility of coating dental implants under an extracorporeal magnetic field with a reduced concentration of PLGA(Ag-Fe_3O_4) to improve biological compatibility without compromising antibacterial efficiency (Scheme 1). The permanent magnet was used to build the magnetic field as close to the PLGA(Ag-Fe_3O_4) as possible. PLGA(Ag-Fe_3O_4) was applied in vivo to the implanted tooth that contained a permanent magnet, allowing for Ag adhesion to the tooth surface without being removed by flushing water. Bacterial infection (such as by *S. mutans*) activates the host immune response to produce reactive oxygen species (ROS), leading to the destruction of the tooth supporting tissues (Scheme 1, left). In the implanted tooth coated with PLGA(Ag-Fe_3O_4), bacterial adhesion was weakened. Thus, the immune system did not produce ROS and the microenvironment around the implanted area stimulated osteoblast proliferation, thus improving the transplant success rate.

Materials and methods

Materials and animals

Silver nitrate ($AgNO_3$), ferric chloride ($FeCl_3{\cdot}6H_2O$), ammonia water ($NH_3{\cdot}H_2O$), and sodium hydroxide (NaOH) were purchased from Xilong Chemical Co, Ltd (Guangxi, China). PLGA (Resomer RG 502H) was purchased from Evonik, Essen, Germany. N-methyl pyrrolidone (NMP, 99%) was purchased from Acros Organics, Geel, Belgium. Trisodium citrate dehydrate ($C_6H_5Na_3O_7{\cdot}2H_2O$) and ferrous chloride ($FeCl_2{\cdot}4H_2O$) were purchased from Shanghai Richjoint Chemical Reagents Co, Ltd (Shanghai, China). Polyvinylpyrrolidone (PVP) was purchased from Shanghai Macklin Biochemical Co, Ltd (Shanghai, China). Agar was purchased from Sunshine Biotechnology Co, Ltd (Nanjing, China).

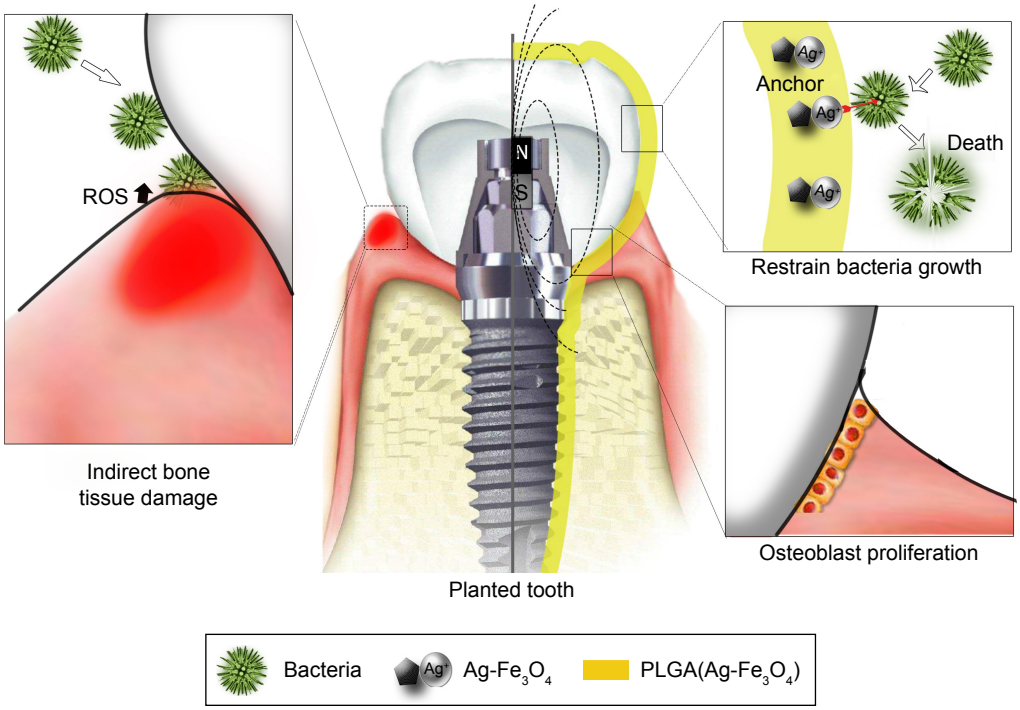

Scheme 1 Schematic diagram of PLGA(Ag-Fe_3O_4)-coated on dental implants.
Notes: Bacterial infection (such as the one by *Streptococcus mutans*) activates host immune response to produce ROS, leading to the destruction of the tooth supporting tissues (left). In the planted tooth (center) covered with PLGA(Ag-Fe_3O_4), bacterial adhesion ability weakened (top right). Thus, the immune system did not produce ROS and the microenvironment around the planted area stimulated osteoblast proliferation and improved the transplant success rate (bottom right).
Abbreviations: PLGA, poly (D, L-lactic-co-glycolic acid); ROS, reactive oxygen species; N, magnetic north pole; S, magnetic south pole.

All other reagents used were of analytical grade. Deionized water was used throughout the experiment.

Specific pathogen-free Sprague–Dawley (SD) rats of both genders (male, 200–215 g; female, 175–190 g) were obtained from the Experimental Animal Center of Nantong University, China. Five rats per cage were housed under controlled environmental conditions (22°C±3°C, 45%–70% relative humidity; 12 hour light/dark cycle). All animal experiments were approved by the Animal Care Committee of Nantong University (including guidelines for animal care and use, and guidelines for euthanasia of rats), which conducted the ethical review of the experiments.

Synthesis of PLGA-coated Ag-Fe_3O_4 nanoparticles

Ag-Fe_3O_4 nanoparticles were prepared by a hydrothermal technique.[22,23] In brief, $FeCl_2 \cdot 4H_2O$ (3.75 mmol) and PVP (20.00 mmol) were dissolved in 150 mL of deionized water. The mixed solution was stirred and heated to 90°C. NaOH solution (10 mL, 1 mol) was added to the mixture. After the mixed solution's temperature reached 90°C, 20 mL of prepared $AgNO_3$ solution (2.5 mmol) and PVP solution (3.75 mmol) were added to the mixture. After stirring for 1 hour, the solution was cooled naturally and washed several times with deionized water and ethyl alcohol absolutely to remove all unreacted impurities.

PLGA (25% w/w, based on the total liquid formulation without drug) was dissolved in NMP at 25°C for 30 minutes under stirring in a glass vial. Ag-Fe_3O_4 was added and the mixture was vortexed for 3 minutes, followed by standing for 3 hours at 25°C.

Ag nanoparticles were prepared as described by Ma et al.[24] In brief, $AgNO_3$ and Na_3 citrate solutions were filtered through a 0.22-μm microporous membrane and nano-Ag was prepared by adding Na_3 citrate solution to boiling $AgNO_3$ aqueous solution.

Characterization

The particle size and distribution of the present samples were studied by transmission electron microscopy (TEM). Measurements were performed using a JEM-200 CX microscope (JEOL, Tokyo, Japan) operated at an accelerating voltage of 80 kV.

X-ray powder diffraction (XRD) measurements were carried out in a D8-ADVANCE (Bruker AXS Inc, Madison, WI, USA) X-ray diffractometer using Cu-Kα radiation.

Fourier transform infrared (FTIR) spectra of the samples were obtained from a Paragon 1000 spectrometer (PerkinElmer Inc, Waltham, MA, USA). The signal resolution of the FTIR was 1 cm^{-1} and a minimum of 16 scans was obtained and averaged within the range of 400–4,000 cm^{-1}.

The magnetic measurement was recorded at room temperature (300 K) by using a vibrating sample magnetometer (LKSM-7410).

To investigate the surface morphology of the planted tooth modified with PLGA(Ag-Fe_3O_4), scanning electron microscopy (SEM) images were obtained on a JSM-6700F microscope (JEOL).[25]

Antibacterial experiment

To evaluate the antibacterial activity against *Streptococcus*, the effect of nano-Ag, Ag-Fe_3O_4, and PLGA(Ag-Fe_3O_4) on the bacterial growth kinetics media was quantitatively studied.[26] The inoculation of bacteria was carried out by growing strains in sheep blood agar plate at 37°C until a level of ~10^9 CFU/mL of bacteria was reached. Then, 0.5 mL of 10^9 CFU/mL bacterial suspension was added to 50 mL lysogeny broth liquid medium-contained teeth modified with nano-Ag, Ag-Fe_3O_4, or PLGA(Ag-Fe_3O_4) with 20 μg/mL Ag and incubated at 37°C. After incubation for 24 hours, the antibacterial efficacy was determined by measuring the OD at 540 nm.

To investigate the stability of antibacterial activity, nano-Ag, Ag-Fe_3O_4, or PLGA(Ag-Fe_3O_4) with 20 μg/mL Ag was incubated in PBS under magnetic stirring (600 rpm); the antibacterial activity was studied after the PBS was changed 2, 4, 6, 8, 10 times.

Bacterial adhesion plate colony count

Approximately 2 mL of bacterial suspension (1×10^9 CFU/L) was co-cultured with teeth modified with nano-Ag, Ag-Fe_3O_4, or PLGA(Ag-Fe_3O_4) with 20 μg/mL Ag for 48 hours. All the samples were then taken out sequentially from the bacterial suspension and rinsed thrice with sterile PBS buffer for 30 seconds to remove non-adherent bacteria. The adherent bacteria were detached ultrasonically from the samples in 10 mL of the same PBS buffer for 5 minutes. After the solution was diluted to a certain factor, 50 mL of washing solution was uniformly coated on the sheep blood agar plate. After the solution was cultured anaerobically for 24 hours, the bacterial colonies were counted.

SEM observation of the surface adhesion of bacteria

After being co-cultured with bacterial suspension and washed, the samples were fixed with a volume fraction of 2.5% glutaraldehyde (Sigma-Aldrich Co, St Louis, MO, USA) for 24 hours at 4°C. The samples were removed and rinsed with sterile PBS buffer thrice, and then dehydrated with 30%, 50%, 70%, 80%, 90%, 100%, and 100% (v/v) graded ethanol, successively, with 15 minutes incubation at each concentration. The samples were dried by a vacuum dryer at a critical point of CO_2 and sprayed with gold coating before the SEM observation.

Stability behavior

In vitro stability behavior of Ag-Fe_3O_4 was tested as follows: Ag-Fe_3O_4 was added to 10 mL PBS (pH 7.4) at 37°C at the concentration of 50 μg/mL. After 2 days, the PBS was placed in a magnetic field, and the concentration in the supernatant was tested. The steps were repeated three times.

The stability of PLGA(Ag-Fe_3O_4) modified on the tooth surface was tested as which was dipped in 20 mL of PBS (pH 7.4) at 37°C with or without the magnetic field; the concentration of Ag in the supernatant was tested for 28 days.

Osteoblasts proliferation assay

Freshly isolated mouse osteoblasts were seeded into 96-well plates at a density of 1×10^4 cells/well in the presence of nano-Ag, Ag-Fe_3O_4, PLGA(Ag-Fe_3O_4), and PLGA(Ag-Fe_3O_4) + M (static magnetic field) (Ag 20 μg/mL). The viability after culture was measured at 24 hours by MTT assay.

ALP activity

For alkaline phosphatase (ALP) activity assessment, using 200 μL of radioimmunoprecipitation assay (RIPA) buffer, the total protein was extracted from osteoblasts cultured with Fe_3O_4 or PLGA(Ag-Fe_3O_4) at days 2, 4, and 6 of the differentiation period. For sedimentation of cell debris, the lysate was centrifuged at 15,000 rpm at 4°C for 15 minutes. After centrifugation, the supernatant was collected, and ALP activity was evaluated with an ALP assay kit (Bomei, Anhui, China). Finally, the enzyme activity (IU/L) was normalized against total protein (mg/dL).

Silver staining for nucleolar organizer region (AgNOR) staining

AgNOR histochemical staining was performed according to the literature.[12] In brief, after 4 days incubation, slides with osteoblasts were fixed in 95% ethanol for 50–60 minutes and then hydrated in distilled water. The silver staining was freshly prepared by dissolving 2% gelatin in 50% aqueous silver nitrate solution in a ratio of 1:2. Slides were incubated for 60 minutes at room temperature in the dark with this solution. After being stained, the slides were rinsed with distilled water, dehydrated with graded ethanol, cleared in xylene,

and coverslipped. The software Image-pro plus 6.0 (Media Cybermetics, Rockville, MD, USA) was used for the analysis according to the manufacturer's instructions.

Blood biochemistry index in vivo

Ten SD rats in each group were employed to evaluate the in vivo blood toxicology behavior. After the modification of nano-Ag, Ag-Fe_3O_4, and PLGA(Ag-Fe_3O_4) on the tooth (implanted with the permanent magnet) for 3 days, liver function markers, including ALP, alanine aminotransferase (ALT), aspartate aminotransferase (AST), the kidney function marker blood urea nitrogen (BUN), as well as creatinine (Cr) and globulin (GLB) were determined by an automated biochemical analyzer (Yoder, Nancy, France). The inflammatory cytokines (superoxide dismutase [SOD] and TNF-α) were analyzed by rat enzyme-linked immunosorbent assay kits.

Statistical analysis

The results were presented as mean ± standard deviation and analyzed using SPSS 13.0 (SPSS Inc, Chicago, IL, USA). The experimental data were examined for equal variance and normal distribution prior to statistical analysis. One-way analysis of variance was used for statistical analysis. Values were considered significantly different if $P<0.05$.

Results

Due to their reduced size, Fe_3O_4 nanoparticles behave as superparamagnets, ie, quasi-static magnetic measurements at room temperature that display the Langevin isotherm without hysteresis.[27] Ag nanoparticles are capable of killing bacteria by directly damaging the cytomembrane, and they are used in cancer therapy and medicine. However, nano-Ag runs off easily from the working point, thus working less effectively. Inspired by this, we demonstrated the safety and efficacy of a dental implant coating to inhibit bacterial proliferation and promote osteoblast proliferation by anchoring nano-Ag on the surface for a long duration.

PLGA(Ag-Fe_3O_4) nanocomposites preparation and characterization

In this study, Ag-Fe_3O_4 was prepared as follows: after the addition of NaOH to $FeCl_2$, $Fe(OH)_2$ was obtained. $AgNO_3$ also reacts with NaOH to form AgOH, and because AgOH is very unstable, it decomposed easily into Ag_2O. Then, the redox reaction between Ag_2O and $Fe(OH)_2$ produces Fe_3O_4 and Ag. Due to high surface energy, the Ag atoms aggregated rapidly, forming nanoparticles as a matrix of the nanocomposites. PVP adsorbed on the Ag nanoparticles surfaces prevented their further growth. In addition, some of the in situ generated Fe_3O_4 particles crystallized with Ag nanoparticles to form Ag-Fe_3O_4 nanocomposites resulting from their strong binding interaction, whereas others adhered to the surface of the nanocomposites. This outcome is in line with the results of previous studies.[22] The reaction process is illustrated by Equations 1–3:

$$3FeCl_2 + 6NaOH = 3Fe(OH)_2 + 6NaCl \quad (1)$$

$$2AgNO_3 + 2NaOH = 2Ag_2O + 2NaNO_3 + H_2O \quad (2)$$

$$3Fe(OH)_2 + Ag_2O = Fe_3O_4 + 2Ag + 3H_2O \quad (3)$$

TEM images of nano-Ag and Ag-Fe_3O_4 are shown in Figure 1A and B. The TEM images of the nano-Ag show its miniscule and regular shape. Ag-Fe_3O_4 morphology consisted of a single-crystal Ag core and polycrystallized Fe_3O_4 shell nanostructures that were amorphous (Figure 1B). Since Fe_3O_4 was bonded with nano-Ag, the size of the Ag-Fe_3O_4 particle was larger than either Fe_3O_4 or nano-Ag alone. Both Ag and Fe_3O_4 nanocrystallites formed composite nanoparticles instead of monocrystals, as demonstrated by the appearance of lattice fringes of the nanoparticles. The high-resolution TEM image (Figure 1C) shows that the nanoparticles comprised both Ag (~0.20 nm, which is consistent with Ag {200} planes of the fcc platinum structure) and Fe_3O_4 (~0.235 nm, which is consistent with Fe_3O_4 {400} planes of the fcc platinum structure) nanocrystallites, forming composite nanoparticles as demonstrated by lattice fringes of the nanoparticles. The PLGA can almost pack the Ag-Fe_3O_4 nanoparticles, and modify the surface of the implant (Figure 1D).

The XRD patterns of Fe_3O_4 and Ag-Fe_3O_4 are shown in Figure 1E. The diffraction peaks located at 30°, 35.4°, 43°, 53.4°, 57°, and 62.6° correspond to the (220), (311), (400), (422), (511), and (440) planes in the Fe_3O_4 cubic lattice; these planes are associated with the spinel structure of magnetite phase (Fe_3O_4, reference JCPDS no. 82-1533). In addition, four peaks were found at 38°, 44°, 65°, and 77°, which represent Bragg reflections of Ag (111), (200), (220), and (311) reflection planes (JCPDS card no. 65-2871). These results are in good agreement with Fe_3O_4 XRD patterns reported in the literature.[28]

To characterize the molecular nature of the material, FTIR spectra of the samples were observed (Figure 1F). The absorption bands at 3,342 and 1,646 cm^{-1} belong to the vibrating peaks of a hydroxyl functional group on the surface of Fe_3O_4 and Ag-Fe_3O_4, indicating that the Ag-Fe_3O_4 composite particles have the same hydroxyl groups as Fe_3O_4. However, the characteristic absorption peak disappeared on the surface of Ag-Fe_3O_4 due to nano-Ag not being characterized by absorption in the infrared region.[29]

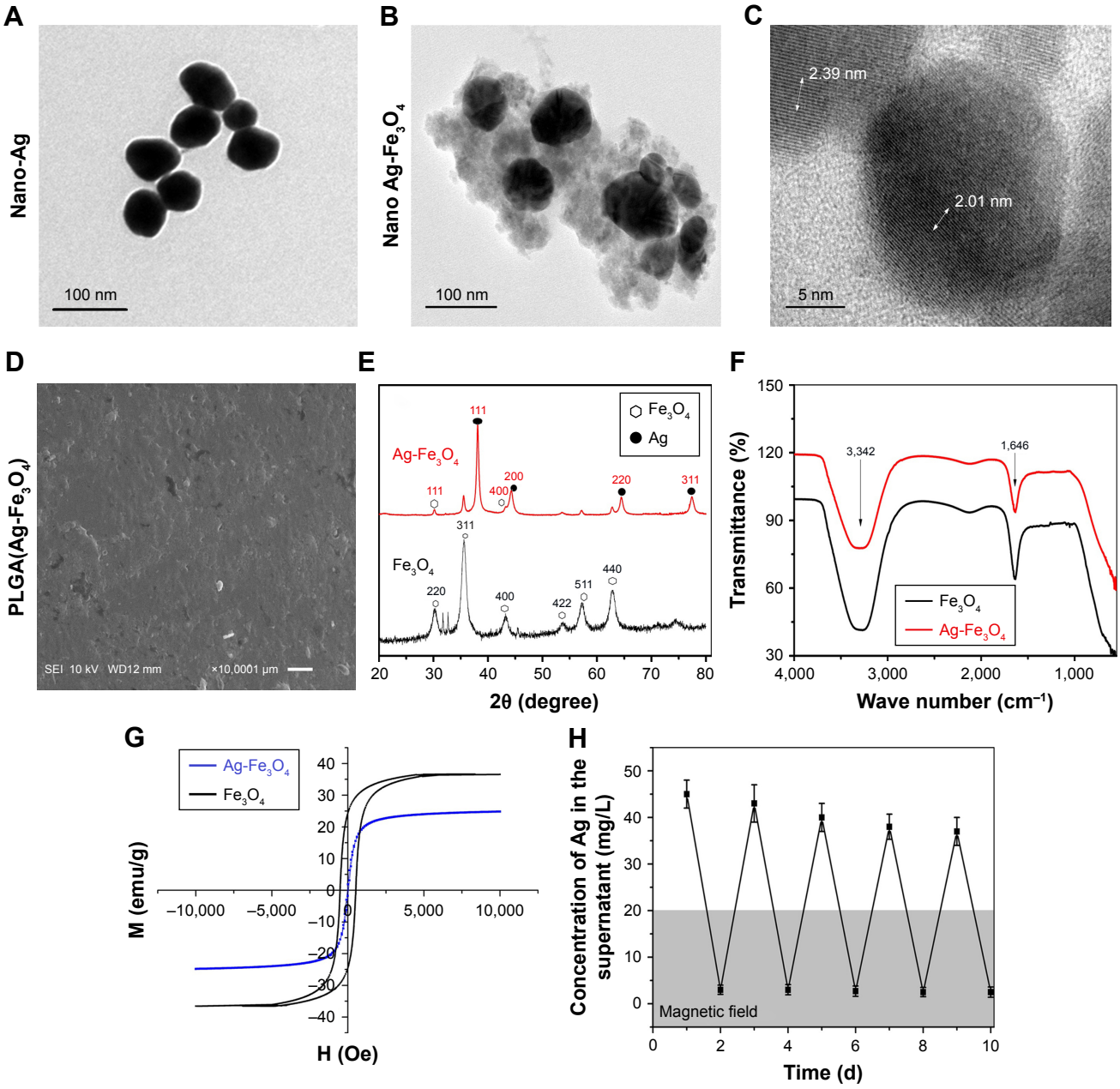

Figure 1 Characterization of PLGA(Ag-Fe_3O_4).

Notes: (**A**) TEM image of Ag nanoparticles. (**B**) TEM image of Ag-Fe_3O_4 nanoparticles. (**C**) HRTEM image. (**D**) SEM image of PLGA(Ag-Fe_3O_4) covered on the planted tooth. (**E**) XRD. (**F**) FTIR spectrum. (**G**) Room temperature magnetic hysteresis loops of Ag-Fe_3O_4. (**H**) Ag-Fe_3O_4 multiple release behavior response to the magnetic field. It meant that Ag was stably bonded with Fe_3O_4.

Abbreviations: PLGA, poly (D, L-lactic-co-glycolic acid); SEI, secondary electron image; TEM, transmission electron microscopy; M, static magnetic field; emu, electromagnetic unit; H, magnetic field strength; Oe, oersted; SEM, scanning electron microscopy; XRD, X-ray powder diffraction; FTIR, Fourier transform infrared; HRTEM, high-resolution transmission electron microscopy; WD, working distance (the distance from the objective lens to focus point).

To evaluate the magnetic response of Ag-Fe_3O_4 to an externally applied magnetic field, magnetization hysteresis curves were obtained by a superconducting quantum interference device (SQUID) magnetometer at 300 K by field cycling between −10 and 10 kOe, as shown in Figure 1G. The magnetic saturation value of Fe_3O_4 nanoparticles was 36.75 emu/g. As Ag connected with Fe_3O_4, a significant decrease in the saturation magnetization of Ag-Fe_3O_4 was observed; specifically, the magnetic saturation value was 23.36 emu/g. Although the composite sample exhibited weak ferromagnetism, there was neither remanence nor coercivity, indicating that the Ag-Fe_3O_4 sample obtained was superparamagnetic. The magnetic recyclability of Ag-Fe_3O_4 was tested in water by placing an external magnet near the glass bottle. The particles were attracted toward the magnet in a few seconds.

Furthermore, Ag-Fe_3O_4 nanoparticles showed long duration stability in vitro. When the Ag-Fe_3O_4 nanoparticles were placed in a magnetic field, the Ag concentration in the

supernatant decreased quickly (Figure 1H). During the next 10 days, the phenomenon was repeated.

PLGA(Ag-Fe_3O_4) antibacterial activity in vitro

To investigate the antibacterial activity of PLGA(Ag-Fe_3O_4) in the mouth, *S. mutans* was chosen as the model bacterium. Bacterial growth kinetics were observed after administration of nano-Ag, Ag-Fe_3O_4, and PLGA(Ag-Fe_3O_4) at the Ag concentration of 20 μg/mL, and the results were determined by measuring the OD at 540 nm. PLGA(Ag-Fe_3O_4) nanoparticles were able to reduce *S. mutans* growth in a similar manner as nano-Ag. The antibacterial action of Ag-Fe_3O_4 was also similar to that of nano-Ag (Figure 2A).

Anchoring the antibiotic material on the tooth surface is the key factor of the efficacy of PLGA(Ag-Fe_3O_4). Figure 2B shows that nano-Ag could not be adsorbed on the tooth surface after washing in the simulation test, while Ag-Fe_3O_4 improved the inhibition rate of *S. mutans* to 31% after being washed 10 times under the magnetic field. The results of

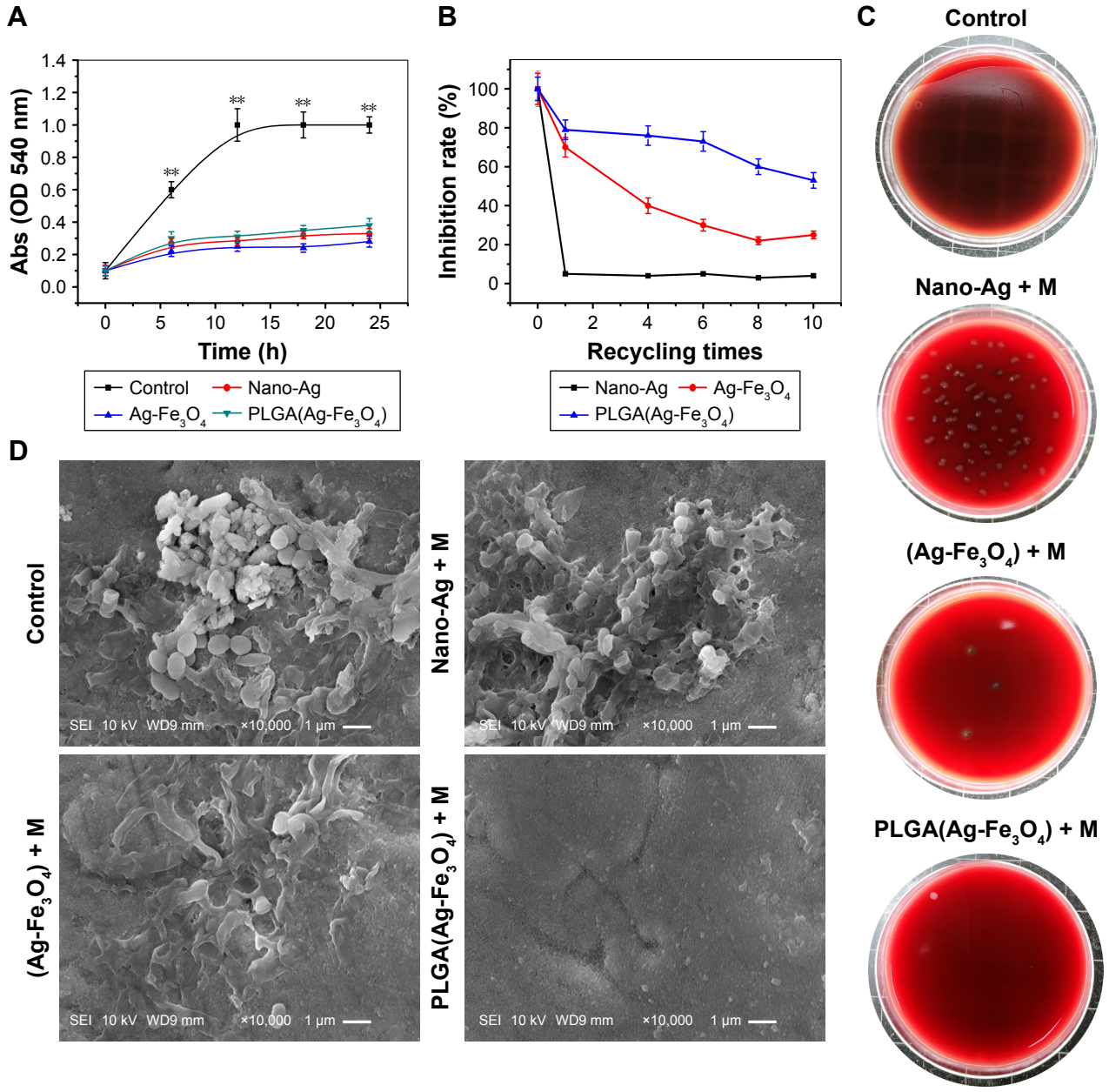

Figure 2 (**A**) Antibacterial results. PLGA(Ag-Fe_3O_4) nanoparticles were able to reduce *Streptococcus mutans* growth as nano-Ag, Ag-Fe_3O_4. $^{**}P<0.01$. (**B**) Antibacterial activity test after washing. PLGA(Ag-Fe_3O_4) under magnetic field can be anchored on the tooth surface and exhibited a long-term antibacterial effect. (**C**) Results of *S. mutans* adhered to the samples surface. (**D**) SEM image of *S. mutans* adhered to the surface of different samples.

Abbreviations: Abs, absorbance; PLGA, poly (D, L-lactic-co-glycolic acid); SEM, scanning electron microscopy; M, static magnetic field; SEI, secondary electron image; WD, working distance (the distance from the objective lens to focus point).

viable bacteria adhering to the different experimental material surfaces are shown in Figure 2C. This indicated that Ag-Fe_3O_4 (Ag ion connects with Fe_3O_4) not only exhibited magnetically recyclable properties but also showed simultaneous antibacterial activity. After modification with PLGA, the inhibition rate increased to 60%, suggesting that PLGA(Ag-Fe_3O_4) remained stable and exhibited bacteriostatic abilities.

SEM observation of the surface adhering bacteria

SEM results of the adherence of *S. mutans* on the samples' surface are shown in Figure 2D. A large number of *S. mutans* colonies adhered on the surface of the tooth covered with nano-Ag, as most of the nano-Ag was washed away. In contrast, the surface of PLGA(Ag-Fe_3O_4)-coated samples under the magnetic field showed very few *S. mutans* colonies.

Osteogenic proliferation test results

When the PLGA(Ag-Fe_3O_4) was modified on the tooth surface, the Ag nanoparticles were stably bonded with Fe_3O_4, and fixed on the tooth for >20 days in vitro (Figure 3A). Measurement of ALP activity was conducted to evaluate the ability of the PLGA(Ag-Fe_3O_4) scaffold to induce osteogenic differentiation (Figure 3B). An analogous increasing trend in ALP activity was observed among the groups. The activity of the enzyme increased as the duration of induction increased. In this regard, osteogenic cells cultured on with Fe_3O_4 and PLGA(Ag-Fe_3O_4) presented higher ALP activity at days 4 ($P<0.05$) and 6 ($P<0.01$), compared with PBS-treated groups.

In Figure 3C, the L_{929} cell line co-cultured with PLGA(Ag-Fe_3O_4) + M at different concentrations showed a high proliferation rate throughout the entire culture incubation time. Cell viability was significantly higher using 100 mg/L PLGA(Ag-Fe_3O_4) + M compared to the other groups ($P<0.01$).

After being stained by a silver impregnation method, the borders of nucleolar organizer regions and the nucleus were clearly visible. The nuclei were stained pale yellow, whereas AgNOR dots or aggregates produced dark staining. As illustrated in Figure 3D, keratinocytes co-cultured with Ag nanoparticles were smaller than the other groups, and fewer AgNOR dots or aggregates were observed. Most of the nuclei in the Ag-Fe_3O_4 group contained one or two AgNORs, while a large number of AgNOR proteins were observed in the PLGA(Ag-Fe_3O_4) and PLGA(Ag-Fe_3O_4) + M groups.

Biochemical detection results

The teeth were treated with the same dose of nano-Ag and PLGA(Ag-Fe_3O_4) + M (the magnetic field was generated by the permanent magnet in the implanted tooth). Liver function markers, including ALP, ALT, and AST, as well as Cr, GLB, and the kidney function marker BUN were also normal during the test procedure (Figure 4A), suggesting no clear hepatic and renal disorders in rats after PLGA(Ag-Fe_3O_4) + M treatment for 3 days. Alternatively, after the nano-Ag treatment, ALP, ALT, and Cr levels were significantly higher than those of the control group ($P<0.05$).

To probe into the causes for those differences, the change of the concentration of silver in the blood was detected. The silver ion passed into the bloodstream and reached the systemic circulation, causing some dose–response toxic side effects. Figure 4B shows that the Ag in the Ag-Fe_3O_4 + M and PLGA(Ag-Fe_3O_4) + M treated groups mainly accumulated in the blood. The silver concentration in the blood did not greatly increase in the PLGA(Ag-Fe_3O_4) + M-treated group; rather, it remained at a relatively low level.

TNF-α and SOD levels were also evaluated after the rats were treated with nano-Ag, Ag-Fe_3O_4, and PLGA(Ag-Fe_3O_4) + M (Figure 4C). Rats treated with PLGA(Ag-Fe_3O_4) + M for 3 days showed less inflammation as indicated by TNF-α and SOD levels that were significantly lower than those in the nano-Ag and Ag-Fe_3O_4 groups. These data suggest that PLGA(Ag-Fe_3O_4) + M is harmless in vivo.

Discussion

It is both a challenge and contradiction to improve biological compatibility without compromising antibacterial activity in a dental implant. Silver, as an excellent antibacterial agent, causes toxicity, including DNA and chromosome damage, due to its accumulation. In spite of its broad spectrum antibacterial activity against various strains of bacteria, widespread use of nano-Ag is still limited. At high concentrations, nanomaterials may compromise cell proliferation since they can easily enter into the cytoplasm and cross the nuclear membrane, implying that the particles can reach the nucleus.[30] Early research reported on the green synthesis of Ag nanoparticles using different biological sources such as plant extracts,[31,32] bacteria,[33] fungi,[34] and enzymes.[35] Nevertheless, the present study is the first to reduce the concentration of nano-Ag on the implanted tooth to improve biosafety without a reduction in antibacterial activity.

A wide spectrum of desirable synergistic and complementary effects can be obtained when the superparamagnetism nanoparticles (Fe_3O_4) are coupled with silver.[23,36] However,

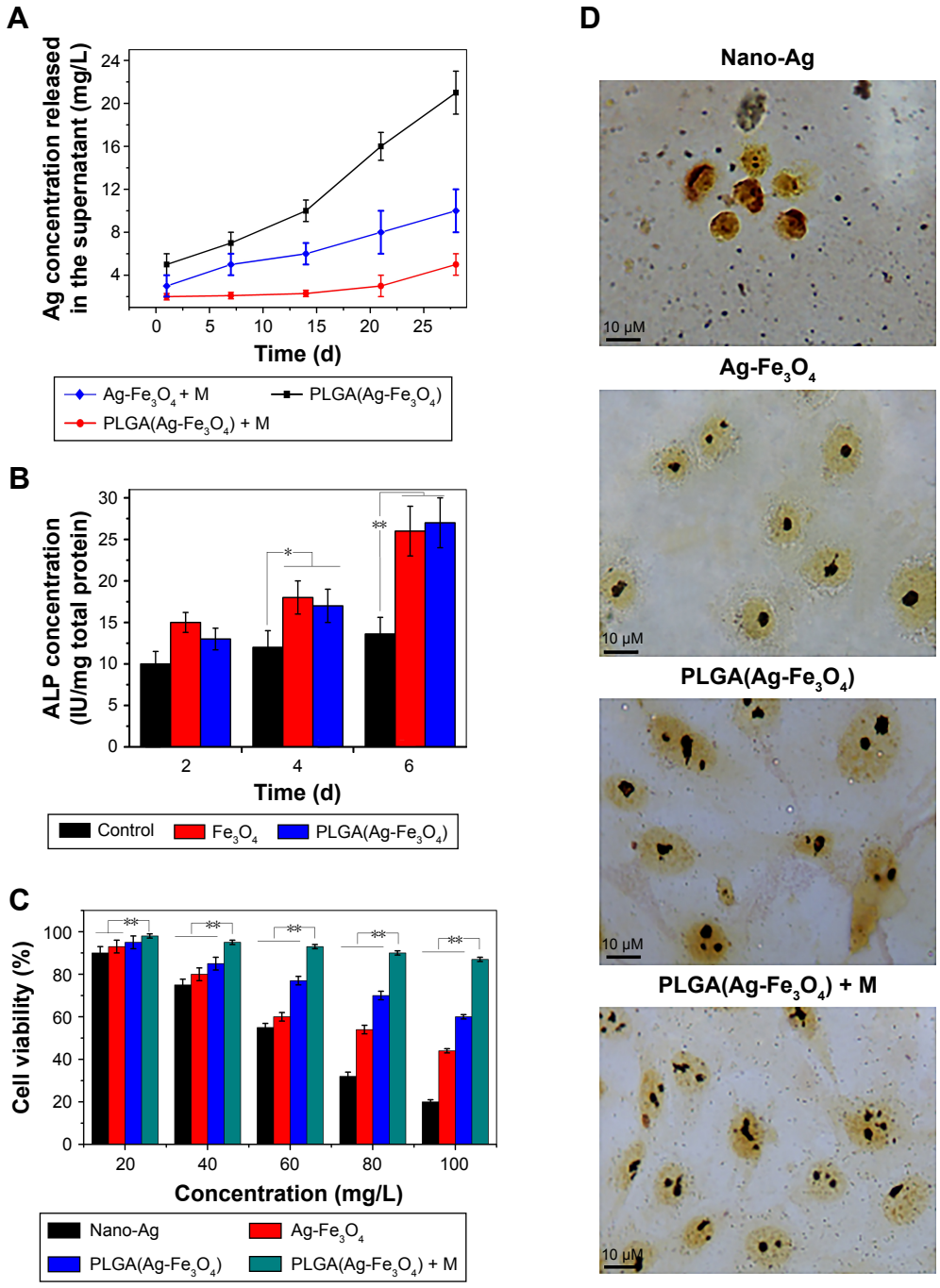

Figure 3 (**A**) Storage stability test result of PLGA(Ag-Fe_3O_4) nanoparticles. (**B**) ALP activity of osteoblasts in PBS, Fe_3O_4, or PLGA(Ag-Fe_3O_4) nanoparticles after 2, 4, and 6 days of differentiation culture; *P<0.05. **P<0.01. (**C**) Viability of osteoblasts incubated with different concentrations of samples for 24 hours. n=6; **P<0.01. (**D**) AgNOR staining in nucleoli of osteoblasts cultured with different nanoparticles. Original magnification 1,000×.

Abbreviations: M, static magnetic field; PLGA, poly (D, L-lactic-co-glycolic acid); ALP, alkaline phosphatase; AgNOR, silver staining for nucleolar organizer region.

the biosafety and efficacy of adherence inhibition involve problems that have yet been solved. In an early study, Prucek et al[37] considered the combination of magnetite nanoparticles and nano silver for use in disinfection and biomedical applications, such as the targeted transport of drugs, as well as for its removal by an external magnetic field. Amarjargal et al[23] reported an enhanced magnetic moment and strong catalytic and antibacterial activities of the Ag-Fe_3O_4 nanocomposite, demonstrating its potential application in water treatment and biomedical applications, with the ability to be subsequently removed by means of an external magnetic field.

The polyester PLGA, which has been approved by Food and Drug Administration for many applications, is biocompatible and biodegradable by hydrolysis of its ester linkages under

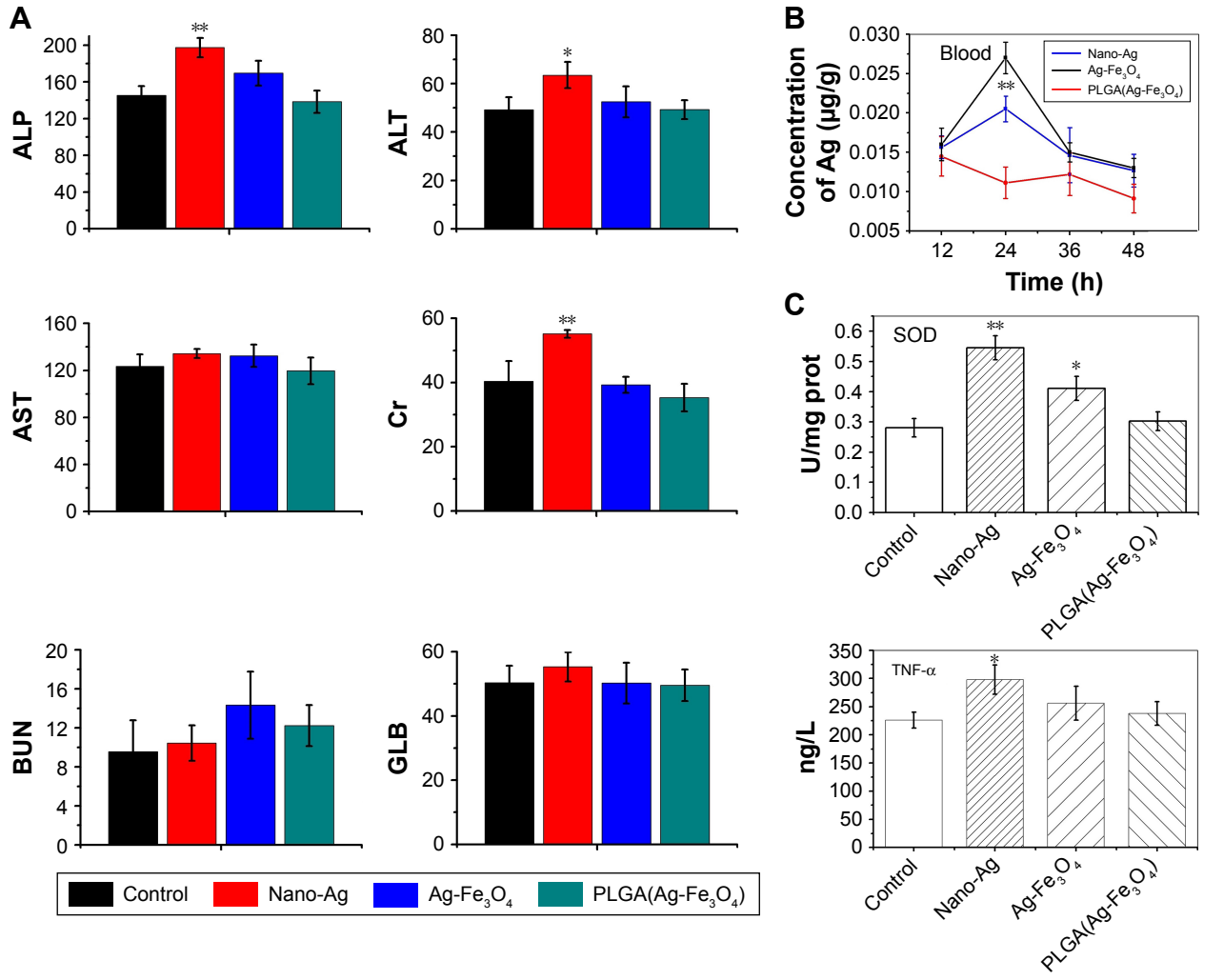

Figure 4 (**A**) Parameters of serum biochemistry profiles after administration of PLGA(Ag-Fe_3O_4) for 3 days. (**B**) The concentration of Ag in blood after treatment with nano-Ag and Ag-Fe_3O_4. Error bars represent standard error (n=5). (**C**) The degree of inflammation factors, including SOD and TNF-α in different samples-treated group. *P<0.05, **P<0.01.

Abbreviations: ALP, alkaline phosphatase; AST, aspartate aminotransferase; BUN, blood urea nitrogen; ALT, alanine aminotransferase; Cr, creatinine; GLB, globulin; PLGA, poly (D, L-lactic-co-glycolic acid); SOD, superoxide dismutase; TNF-α, tumor necrosis factor-α.

physiological conditions and is excreted from the body as carbon dioxide and water via the Krebs cycle.[38] In this study, we developed a coated PLGA(Ag-Fe_3O_4)-implanted tooth obtained under an extracorporeal magnetic field that used a modest concentration of this nanoparticle. TEM, XRD, and FTIR results showed that Ag was connected to the surface of the Fe_3O_4 particle. Ag-Fe_3O_4 nanoparticles were well dispersed and did not agglomerate easily. Results for several analyses of broad spectrum antibacterial activity of the nano-Ag revealed that various bacterial strains died upon contact with the silver iron. The antibacterial effect of Ag-Fe_3O_4 could thus be attributed to the silver ions. In addition, Ag-Fe_3O_4 showed good magnetic properties through its magnetic saturation value that was less than that of Fe_3O_4. Ag-Fe_3O_4 with antibacterial activity and good magnetic properties might be used in biomedicine. In this study, since a permanent magnet was implanted in the implant tooth, few Ag-Fe_3O_4 nanoparticles were washed away in the magnetic field.

Controlling bacterial burden is currently one of the most important problems in the implanted gum preparation.[39] In clinical practice, antibacterial agents are used in high dose to prevent infection, leading to low biosafety. Thus, "antibacterial" and "biosafety" seem to represent an irreconcilable contradiction. Bacterial infections such as those due to *S. mutans* lead to the host immune response to produce ROS, consequently leading to the destruction of the tooth supporting tissues. One of the purposes of this study was to control inflammation and promote osteoblast proliferation.

PLGA(Ag-Fe_3O_4) was adopted to improve biological compatibility without compromising bacteriostatic efficiency. When the nano-Ag is firmly bonded with Fe_3O_4, it can

significantly increase the concentration of the drug in the treatment site and hence decrease the drug dosage. As Ag-Fe_3O_4 was applied to the implanted tooth, the use of a magnetic field anchored the Ag to the tooth surface, making it resistant to flushing water. When the implanted tooth was covered with PLGA(Ag-Fe_3O_4), the bacterial adhesion ability weakened. Thus, the immune system did not produce ROS, and the microenvironment of the implanted area stimulated osteoblast proliferation, which increased the success rate of the dental implant.

According to our results, nano-Ag was stably anchored onto the surface of the tooth in the PLGA(Ag-Fe_3O_4) + M-treated group. The antibacterial effect of PLGA(Ag-Fe_3O_4) + M was significantly higher than that of the nano-Ag group after washing six times. Further, less *S. mutans* adhesion was observed on the tooth surface, indicating that anchoring the silver on the tooth surface is an effective method to prevent bacterial infections.

Acute and chronic nano-Ag exposure causes remarkable damages in various organs, such as the liver and kidney.[40] Since liver injury occurs due to the cumulative nano-Ag effect, and a dose–response relationship exists, effective protection from such damage can be obtained by reducing the concentration used. Despite using the same Ag concentration, the Ag level on the tooth surface in PLGA(Ag-Fe_3O_4) + M was significantly higher than that of the nano-Ag. Alternatively, the Ag level in the blood and liver was higher with nano-Ag than with PLGA(Ag-Fe_3O_4) + M. Further, in this study, the concentration of silver iron in the liver and kidney of the PLGA(Ag-Fe_3O_4) + M group was significantly lower than the concentration in the nano-Ag group. The serum biochemical parameter results showed that PLGA(Ag-Fe_3O_4) + M resulted in no damage to the liver. SOD and TNF-α results showed that nano-Ag caused remarkably more liver and kidney damage than PLGA(Ag-Fe_3O_4) + M. Hence, the present results showed that PLGA(Ag-Fe_3O_4) + M exhibited magnetic properties without losing antimicrobial properties, leading to minimal side effects.

Conclusion

This work analyzed the ability of nano-Ag to improve biological compatibility without compromising antibacterial activity. PLGA(Ag-Fe_3O_4) + M showed the best combination in terms of magnetic properties, antibacterial ability, and osteoblast-promoted proliferation and thus might represent another important and promising application. Therefore, this work provides experimental evidence for further clinical research to improve antibacterial action, reducing the unwanted side effects and improving antibacterial activity.

Acknowledgments

This work was supported by the National Natural Science Foundation of China (nos. 51472115 and 81570952), the Scientific Research Foundation of Graduate School of Nanjing University (no. 2016CL13), the Jiangsu Province Natural Science Foundation of China (nos. BK 20170143, BK20161114), and the Medical Science and Technology Development Foundation, Nanjing Department of Health (nos. ZKX16054, ZKX13050). Major Project supported by Medical Science and Technology Development Foundation, Nanjing Department of Health (no. ZDX16008).

Disclosure

The authors report no conflicts of interest in this work.

References

1. Perry DA, Beemsterboer P, Essex G. *Periodontology for the Dental Hygienist*. 4th ed. St Louis: Elsevier/Saunders; 2014.
2. Schwach-Abdellaoui K, Vivien-Castioni N, Gurny R. Local delivery of antimicrobial agents for the treatment of periodontal diseases. *Eur J Pharm Biopharm*. 2000;50(1):83–99.
3. Christodoulides M. *Neisseria Meningitidis: Advanced Methods and Protocols*. New York: Humana Press, Springer; 2012.
4. Sanchez MC, Llama Palacios A, Fernández E, et al. An in vitro biofilm model associated to dental implants: structural and quantitative analysis of in vitro biofilm formation on different dental implant surfaces. *Dent Mater*. 2014;30(10):1161–1171.
5. Kolenbrander PE, editor. *Oral Microbial Communities: Genomic Inquiry and Interspecies Communication*. Washington, DC: ASM Press; 2011.
6. National Caries Program (US), American Society for Microbiology. *Streptococcus mutans and Dental Caries: Proceedings of a Round Table Discussion*. 73rd Annual Meeting, American Society for Microbiology, Miami Beach, Florida, May 10, 1973. DHEW publication no (NIH) 75-286. Bethesda, MD, USA: US Dept of Health, Education, and Welfare, Public Health Service, National Institutes of Health; 1975.
7. Remaut H, Fronzes RM. *Bacterial Membranes: Structural and Molecular Biology*. Norfolk: Caister Academic Press; 2014.
8. Ducry L, editor. *Antibody-Drug Conjugates*. New York: Humana Press, Springer; 2013.
9. Bush K, editor. *Antimicrobial Therapeutics Reviews: The Bacterial Cell Wall as an Antimicrobial Target*. Boston, MA: Blackwell; 2013.
10. Dibrov P, Dzioba J, Gosink KK, Häse CC. Chemiosmotic mechanism of antimicrobial activity of Ag(+) in Vibrio cholerae. *Antimicrob Agents Chemother*. 2002;46(8):2668–2670.
11. Bala T, Armstrong G, Laffir F, Thornton R. Titania-silver and alumina-silver composite nanoparticles: novel, versatile synthesis, reaction mechanism and potential antimicrobial application. *J Colloid Interface Sci*. 2011;356(2):395–403.
12. Chrastina A, Schnitzer JE. Iodine-125 radiolabeling of silver nanoparticles for in vivo SPECT imaging. *Int J Nanomedicine*. 2010;5:653–659.
13. Chakraborty I, Udayabhaskararao T, Pradeep T. High temperature nucleation and growth of glutathione protected ~Ag75 clusters. *Chem Commun (Camb)*. 2012;48(54):6788–6790.
14. Ding W, Guo L. Immobilized transferrin Fe_3O_4@SiO_2 nanoparticle with high doxorubicin loading for dual-targeted tumor drug delivery. *Int J Nanomedicine*. 2013;8:4631–4639.
15. Muniz-Miranda M, Gellini C, Giorgetti E, Margheri G. Bifunctional Fe_3O_4/Ag nanoparticles obtained by two-step laser ablation in pure water. *J Colloid Interface Sci*. 2017;489:100–105.

16. Li G, Shen B, He N, Ma C, Elingarami S, Li Z. Synthesis and characterization of Fe_3O_4@SiO_2 core-shell magnetic microspheres for extraction of genomic DNA from human whole blood. *J Nanosci Nanotechnol*. 2011;11(12):10295–10301.
17. Vincenzini P, Mitic VV. *Advances in Electrical and Magnetic Ceramics: Proceedings of the 12th International Ceramics Congress, Part F, Part of CIMTEC 2010 – 12th International Ceramics Congress and 5th Forum on New Materials, Montecatini Terme, Italy, June 6–11, 2010*. Advances in science and technology (Faenza, Italy). Stafa-Zuerich, Enfield, NH: Trans Tech Publications Ltd; 2011.
18. Wang C, Zhang K, Zhou Z, et al. Vancomycin-modified Fe_3O_4@SiO_2@Ag microflowers as effective antimicrobial agents. *Int J Nanomedicine*. 2017;12:3077–3094.
19. Meng J, Zhang Y, Qi X, et al. Paramagnetic nanofibrous composite films enhance the osteogenic responses of pre-osteoblast cells. *Nanoscale*. 2010;2(12):2565–2569.
20. Jimenez-Rodriguez RM, Ciuro FP, Padillo J. Authors' reply: a new technique to close open abdomen using negative pressure therapy and elastic gums. *Injury*. 2016;47(11):2602.
21. Liu J, Xu J, Zhou J, Zhang Y, Guo D, Wang Z. Fe_3O_4-based PLGA nanoparticles as MR contrast agents for the detection of thrombosis. *Int J Nanomedicine*. 2017;12:1113–1126.
22. Zhu S, Fan C, Wang J, He J, Liang E, Chao M. Realization of high sensitive SERS substrates with one-pot fabrication of Ag-Fe_3O_4 nanocomposites. *J Colloid Interface Sci*. 2015;438:116–121.
23. Amarjargal A, Tijing LD, Im IT, Kim CS. Simultaneous preparation of Ag/Fe_3O_4 core-shell nanocomposites with enhanced magnetic moment and strong antibacterial and catalytic properties. *Chem Eng J*. 2013;226:243–254.
24. Ma Z, Dong G, Peng M, Tan D, Zhang L, Qiu J. Fabrication of silica nano/micro-fibers doped with one-dimensional assembly of silver nanoparticles. *J Nanosci Nanotechnol*. 2013;13(1):325–332.
25. Briones E, Colino CI, Lanao JM. Study of the factors influencing the encapsulation of zidovudine in rat erythrocytes. *Int J Pharm*. 2010;401(1–2):41–46.
26. Li WH, Yang N. Green and facile synthesis of Ag–Fe_3O_4 nanocomposites using the aqueous extract of Crataegus pinnatifida leaves and their antibacterial performance. *Mater Lett*. 2016;162:157–160.
27. Bear JC, Patrick PS, Casson A, et al. Magnetic hyperthermia controlled drug release in the GI tract: solving the problem of detection. *Sci Rep*. 2016;6:34271.
28. Jiang W, Zhou Y, Zhang Y, Xuan S, Gong X. Superparamagnetic Ag@Fe_3O_4 core-shell nanospheres: fabrication, characterization and application as reusable nanocatalysts. *Dalton Trans*. 2012;41(15):4594–4601.
29. Wang T, Zhang L, Su Z, Wang C, Liao Y, Fu Q. Multifunctional hollow mesoporous silica nanocages for cancer cell detection and the combined chemotherapy and photodynamic therapy. *ACS Appl Mater Interfaces*. 2011;3(7):2479–2486.
30. Lu S, Xia D, Huang G, Jing H, Wang Y, Gu H. Concentration effect of gold nanoparticles on proliferation of keratinocytes. *Colloids Surf B Biointerfaces*. 2010;81(2):406–411.
31. Ulug B, Haluk Turkdemir M, Cicek A, Mete A. Role of irradiation in the green synthesis of silver nanoparticles mediated by fig (Ficus carica) leaf extract. *Spectrochim Acta A Mol Biomol Spectrosc*. 2015;135:153–161.
32. Abdel-Aziz MS, Abou-El-Sherbini KS, Hamzawy EM, Amr MH, El-Dafrawy S. Green synthesis of silver nano-particles by Macrococcus bovicus and its immobilization onto montmorillonite clay for antimicrobial functionality. *Appl Biochem Biotechnol*. 2015;176(8):2225–2241.
33. Chowdhury S, Basu A, Kundu S. Green synthesis of protein capped silver nanoparticles from phytopathogenic fungus Macrophomina phaseolina (Tassi) Goid with antimicrobial properties against multidrug-resistant bacteria. *Nanoscale Res Lett*. 2014;9(1):365.
34. Hamedi S, Shojaosadati SA, Shokrollahzadeh S, Hashemi-Najafabadi S. Extracellular biosynthesis of silver nanoparticles using a novel and non-pathogenic fungus, Neurospora intermedia: controlled synthesis and antibacterial activity. *World J Microbiol Biotechnol*. 2014;30(2):693–704.
35. Willner I, Basnar B, Willner B. Nanoparticle-enzyme hybrid systems for nanobiotechnology. *FEBS J*. 2007;274(2):302–309.
36. Ghaseminezhad SM, Shojaosadati SA, Meyer RL. Ag/Fe_3O_4 nanocomposites penetrate and eradicate S. aureus biofilm in an in vitro chronic wound model. *Colloids Surf B Biointerfaces*. 2018;163:192–200.
37. Prucek R, Tuček J, Kilianová M, et al. The targeted antibacterial and antifungal properties of magnetic nanocomposite of iron oxide and silver nanoparticles. *Biomaterials*. 2011;32(21):4704–4713.
38. Stachewicz U, Qiao T, Rawlinson SCF, et al. 3D imaging of cell interactions with electrospun PLGA nanofiber membranes for bone regeneration. *Acta Biomater*. 2015;27:88–100.
39. Douglass J. Wound bed preparation: a systematic approach to chronic wounds. *Br J Community Nurs*. 2003;8(6 Suppl):S26–S34.
40. Hamilton RF, Buckingham S, Holian A. The effect of size on Ag nanosphere toxicity in macrophage cell models and lung epithelial cell lines is dependent on particle dissolution. *Int J Mol Sci*. 2014;15(4):6815–6830.